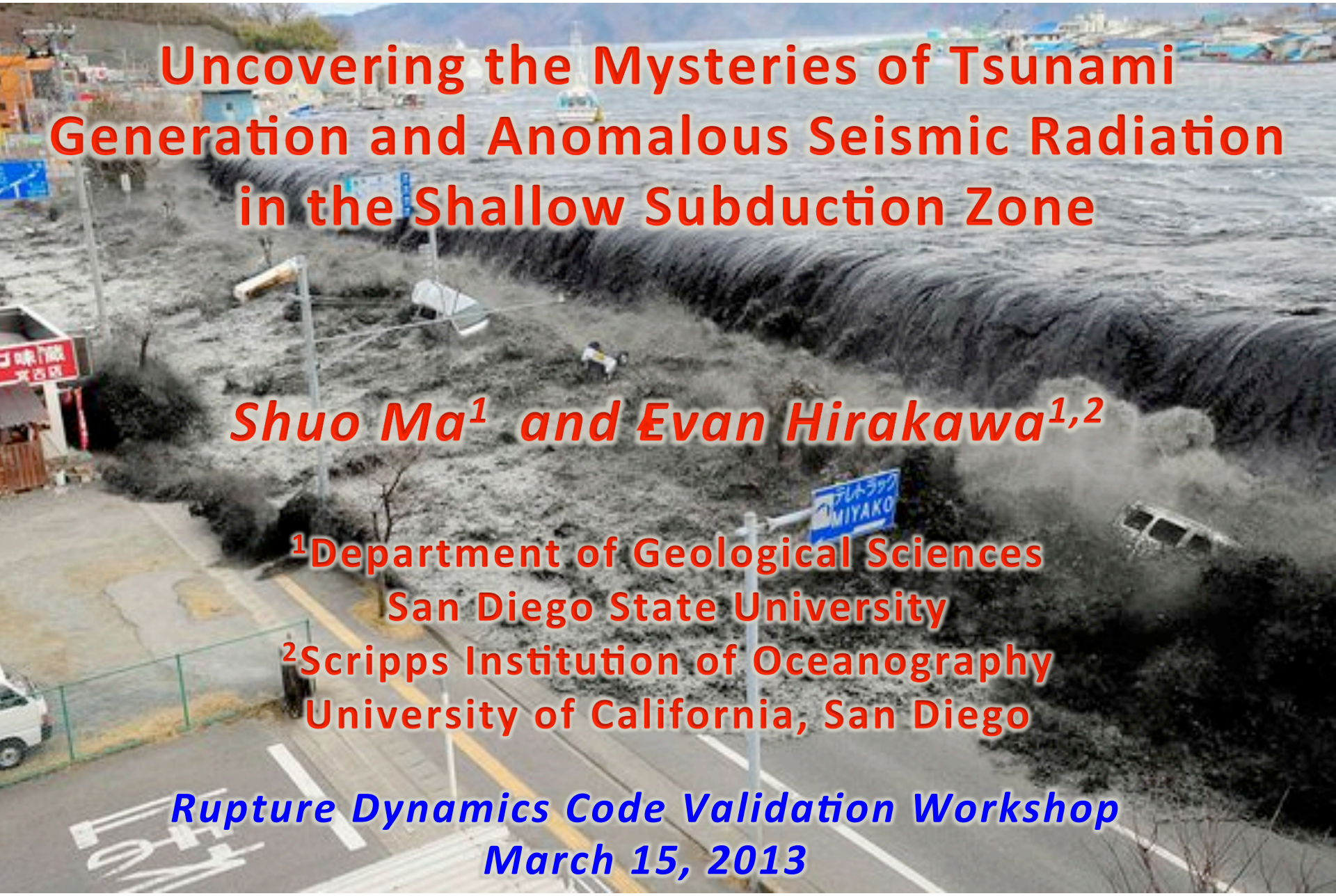

Uncovering the Mysteries of Tsunami Generation and Anomalous Seismic Radiation in the Shallow Subduction Zone

Shuo Ma[1] and Evan Hirakawa[1,2]

[1]Department of Geological Sciences
San Diego State University
[2]Scripps Institution of Oceanography
University of California, San Diego

Rupture Dynamics Code Validation Workshop
March 15, 2013

40-Year Puzzles About Tsunami Earthquakes

Identified by Hiroo Kanamori in 1972

- Large tsunamis
- Depletion in high-frequency radiation

- Slow rupture velocity and long rupture duration

- Possibly small stress drop and slip velocity

- Low energy-to-moment ratio

- Occur in a frictionally stable (velocity-strengthening) or conditionally stable regime

Characteristics of Large Tsunamigenic Earthquakes

- Weak high-frequency radiation
- Slow rupture velocity (long rupture duration)
- Strong tsunami generation

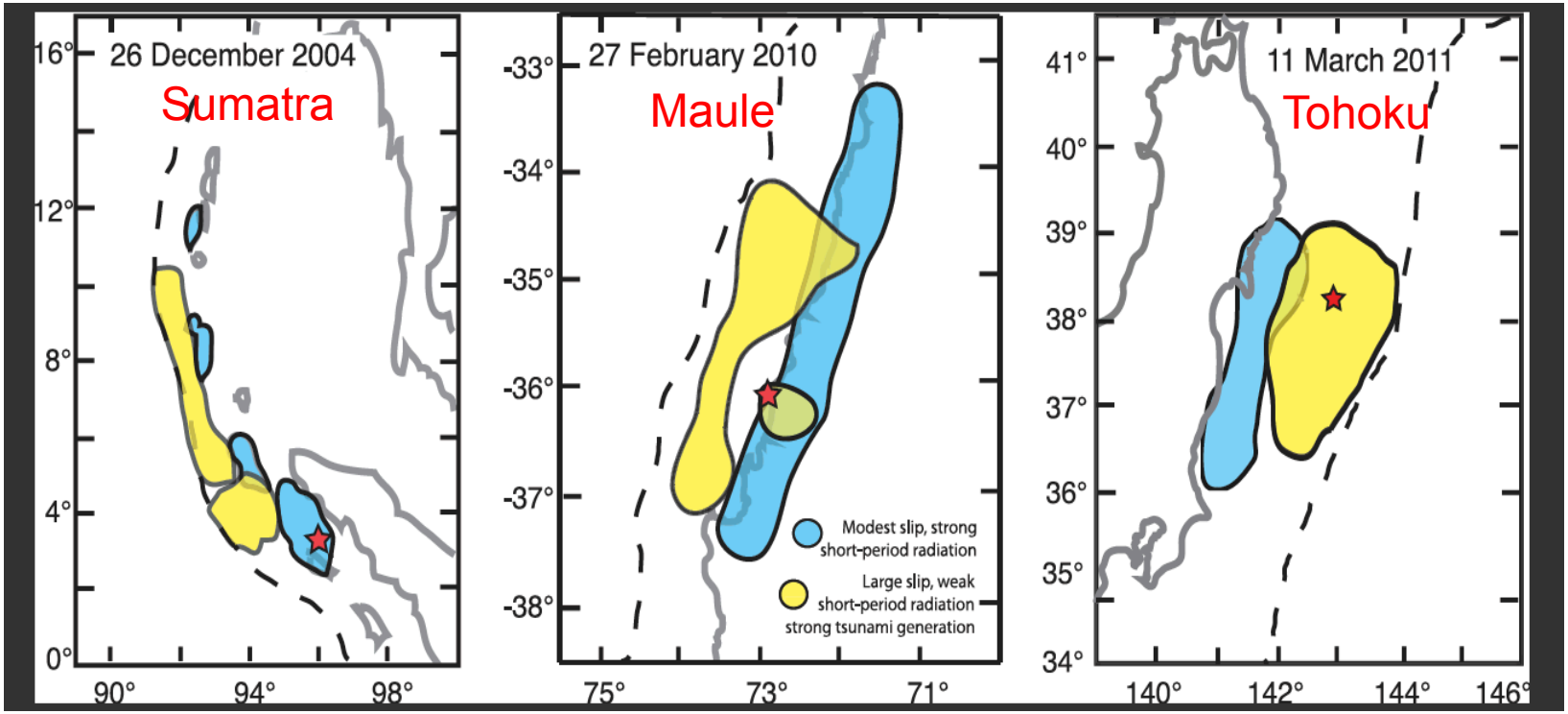

Lay et al. (2012)

Mechanism for Slow Rupture Propagation: Sediments and Fault Morphology

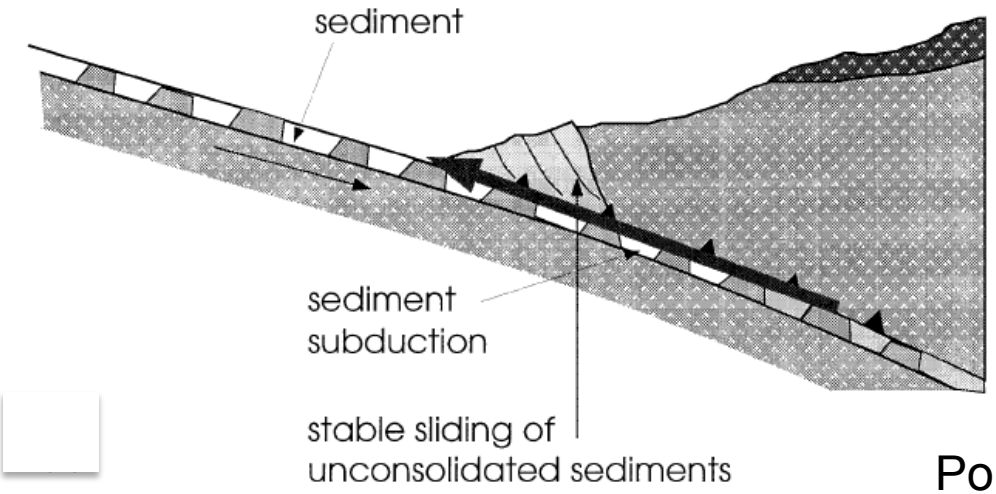

Polet and Kanmori (2000)

- Presence of sediments gives rise to slow rupture velocity.
- Horst-and-graben structure on the plate interface allows the rupture to reach the trench.
- Fault roughness causes large fracture energy.

One inconsistency:
Fault roughness tends to generate more high-frequency radiation.

Dynamic Rupture Simulations in a Low-Velocity Fault Zone

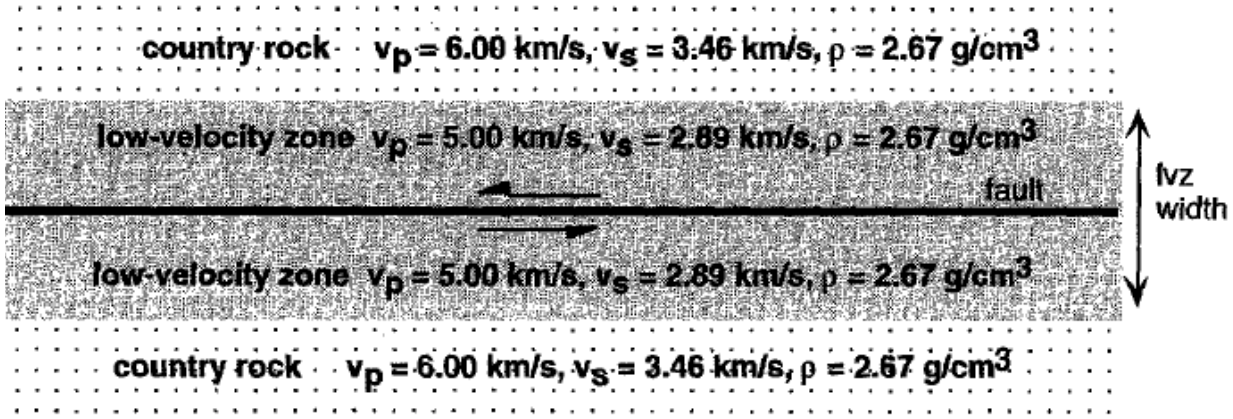

Harris and Day (1997)

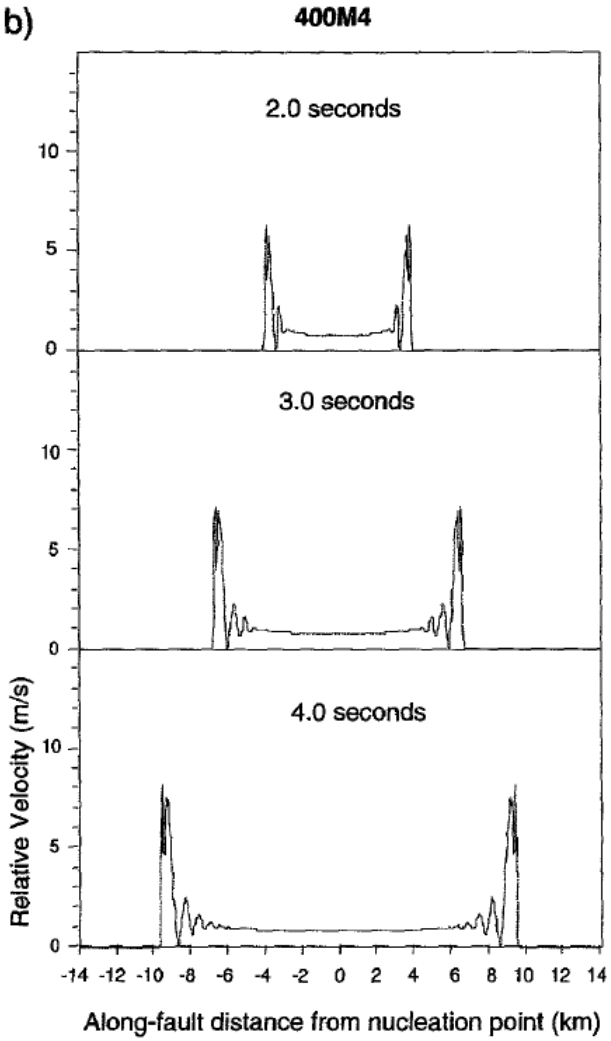

Sediments in the fault zone:

- Promote pulse-like rupture.
- Do not always decrease rupture velocity, and can instead lead to supershear rupture.

More high-frequency radiation!

Mechanism for Tsunami Generation: Large Shallow Slip

Nearly horizontal displacement

Inefficient to generate tsunami

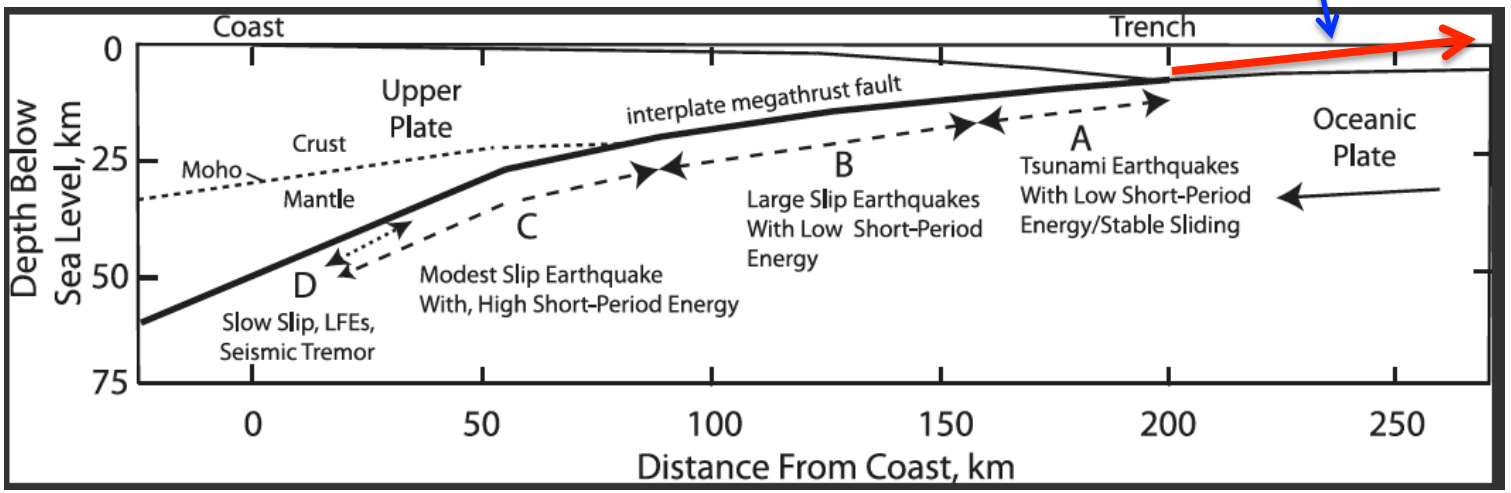

Lay et al. (2012)

$$\text{uplift} \approx \text{slip} \times \sin(\text{dip})$$

Shallow fault dip $\xrightarrow{?}$ large slip

Slip Models Using Tsunami Data

Sumatra

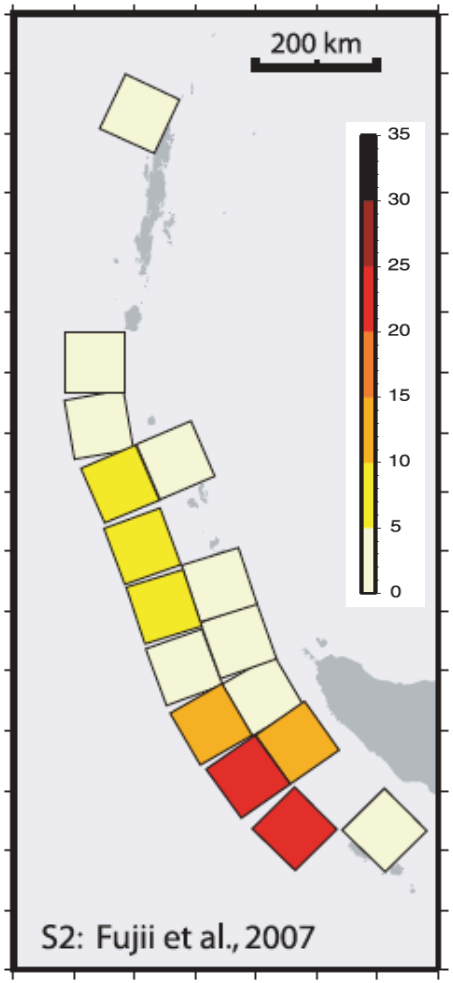

Fujii et al. (2007)

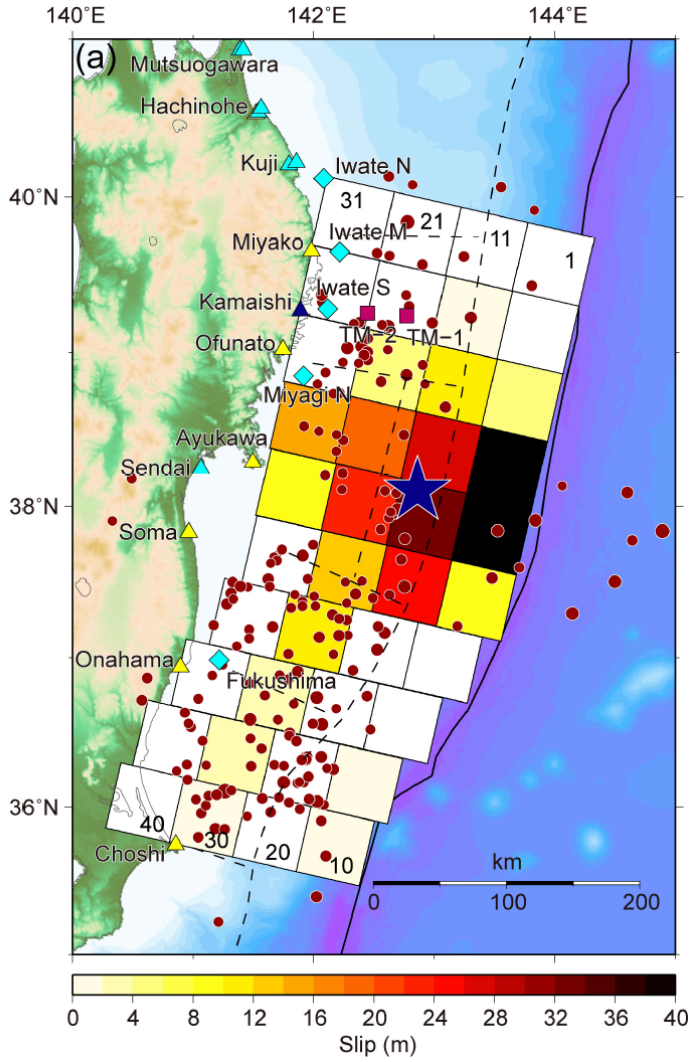

Tohoku

Fujii et al. (2011)

Tohoku Slip Models Using Teleseismic or GPS Data

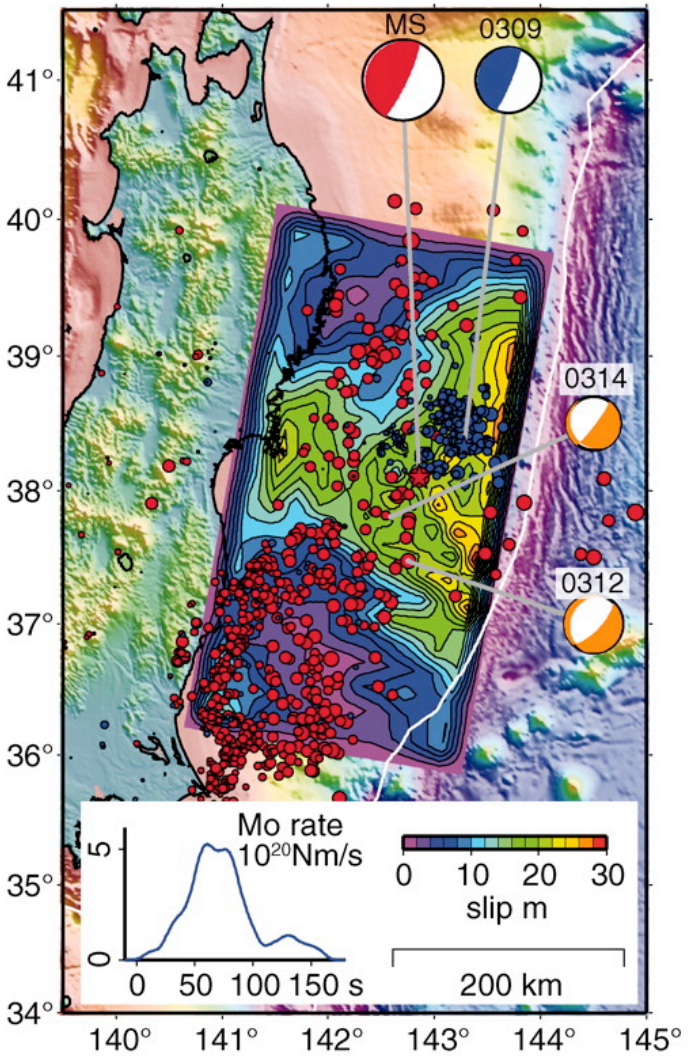

Ide et al. (2011)

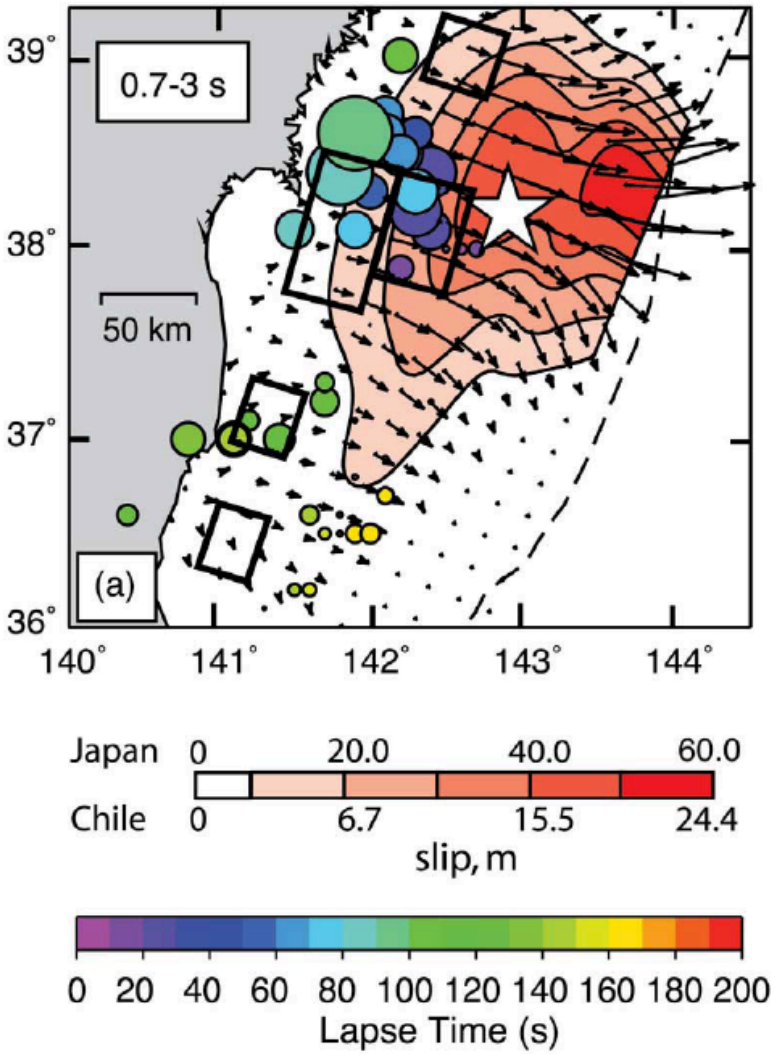

Lay et al. (2012)

Critical Taper (Coulomb Wedge) Theory

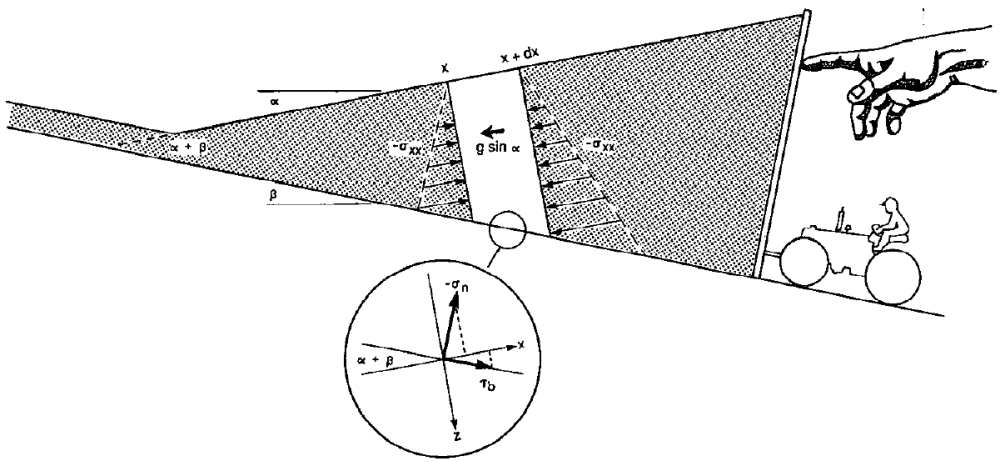

"The overall mechanics of fold-and-thrust belts and accretionary wedges along compressive plate boundaries is considered to be analogous to that of a wedge of soil or snow in front of a moving bulldozer… The critical taper is the shape for which the wedge is on the verge of failure under horizontal compression everywhere, including the basal decollement."

Davis et al. (1983)

Fault Geometry and Stress Conditions

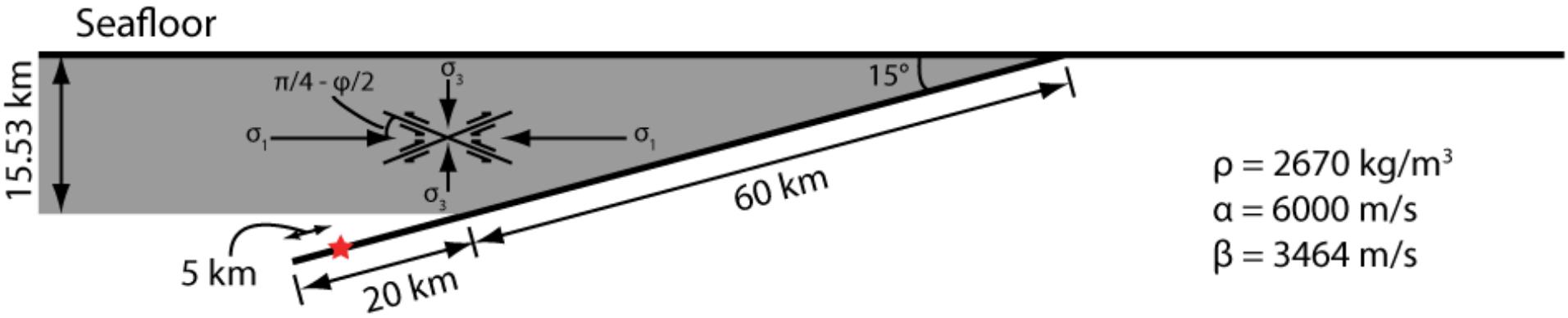

Depth-dependent effective stresses:

$$\sigma_3 = \sigma_{zz} = -(1-\lambda)\rho g z$$

$$\sigma_1 = \sigma_{xx} = 3.7469\ \sigma_{zz}$$

$$\mu_0 = \tau / \sigma_N = 0.58$$

Mohr-Coulomb Failure Criterion

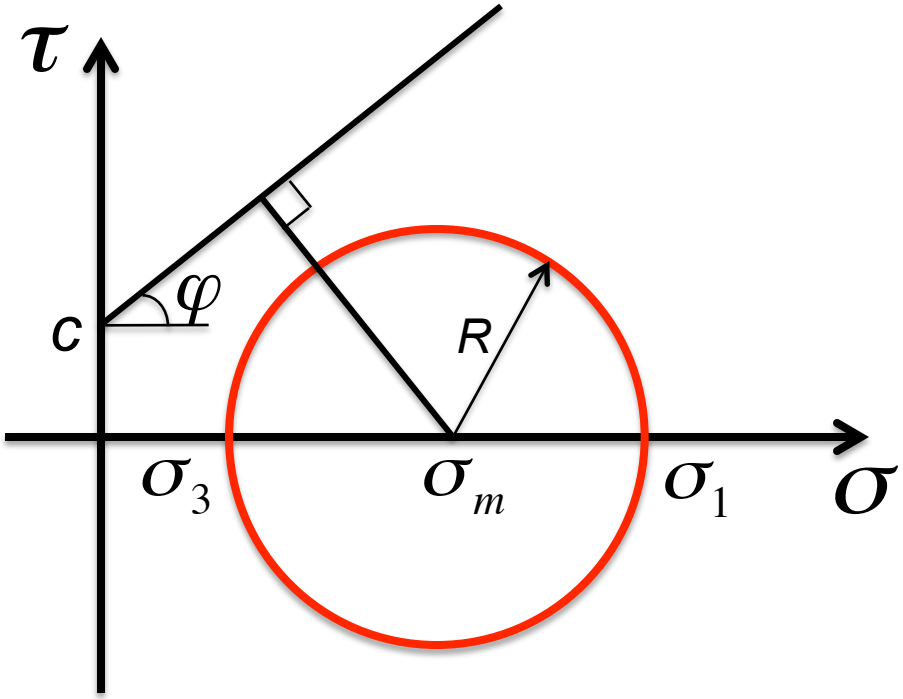

Closeness-to-Failure (*CF*)

$$CF = \frac{R}{c\cos\varphi - \sigma_m \sin\varphi}$$

$$c = 0.017\sigma_{zz}$$
$$\tan\varphi = 0.7095$$

CF = 0.99

Sub-critical wedge

Slip-Weakening Friction

The fault is also close to failure.

$\mu_s = 0.6$ $\quad \mu_0 = 0.58$

$\mu_d = 0.57$ $\quad D_c = 0.2$ m

$$S = \frac{\mu_s - \mu_0}{\mu_0 - \mu_d} = 2$$

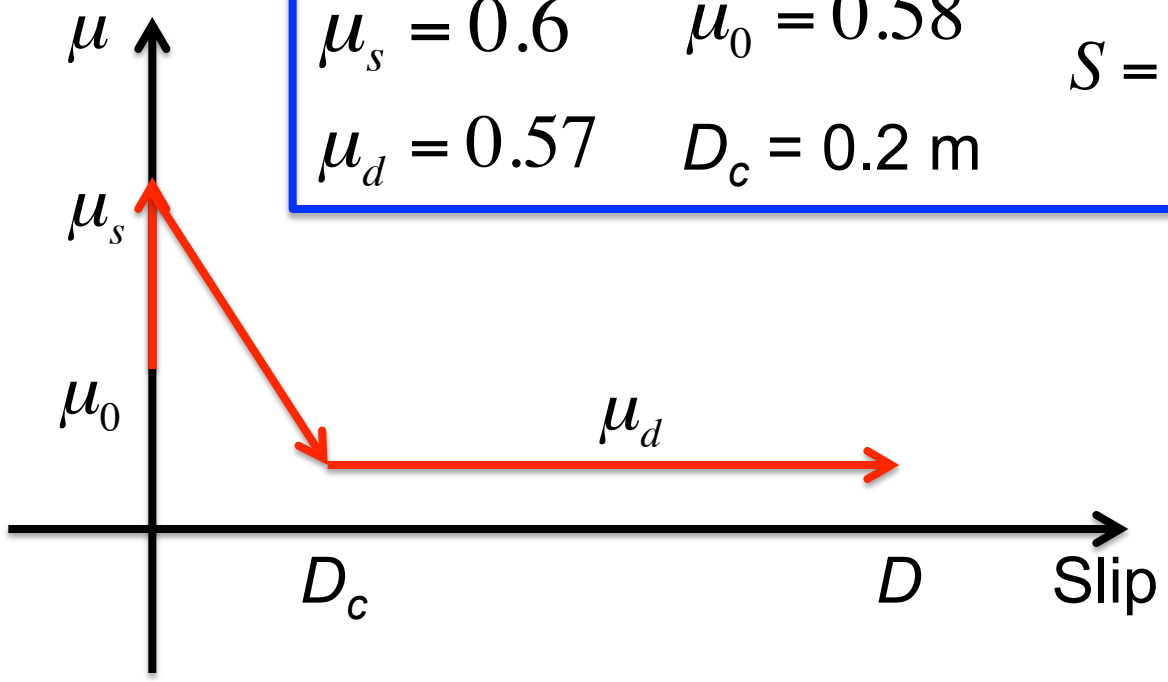

Ida (1972)

No velocity-strengthening friction is used.

Pore Pressure Change in Undrained Condition

$$\Delta p = B\frac{1+\nu_u}{3}(\Delta\sigma_{xx} + \Delta\sigma_{zz})$$

B: Skempton's coefficient

ν_u :undrained Poisson's ratio

We use *B* = 0.3 everywhere in the wedge.

Rupture Movie (Hydrostatic)

Time-Distance Plots of Slip Velocity and Slip Distribution (Red)

Elastic

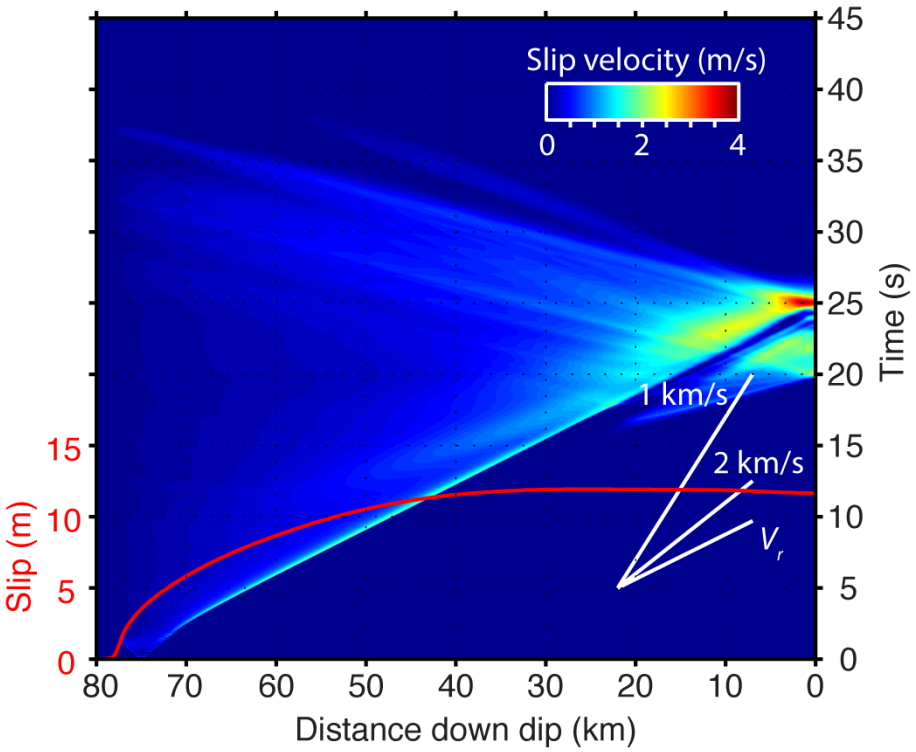

Large rupture velocity
Large slip near the trench

Inelastic

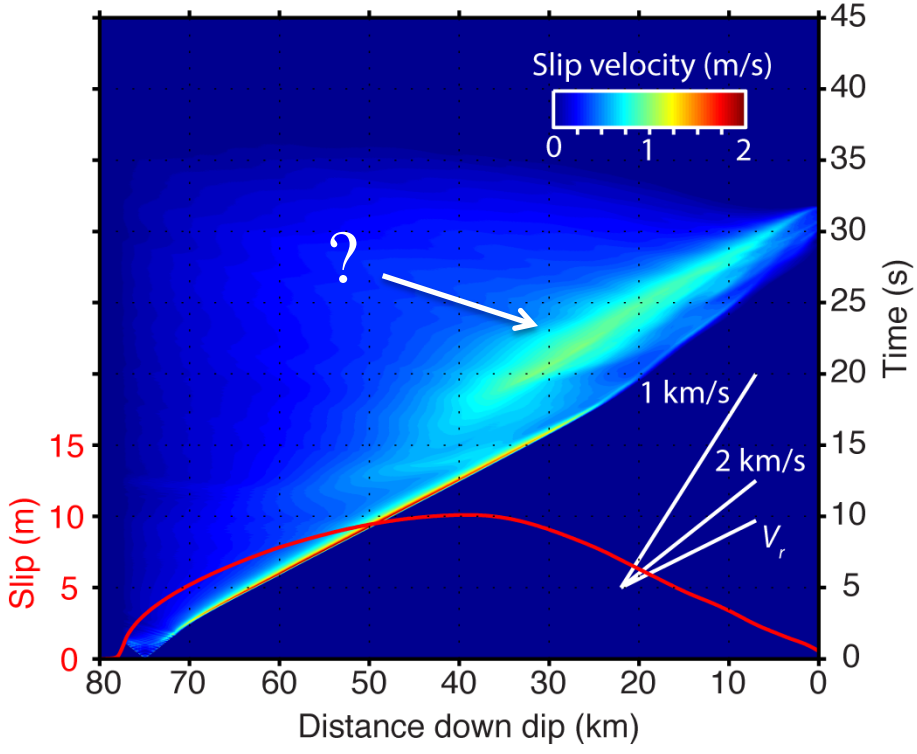

Slow rupture velocity
Small slip near the trench

Time Histories at 25 km and 65 km Down Dip

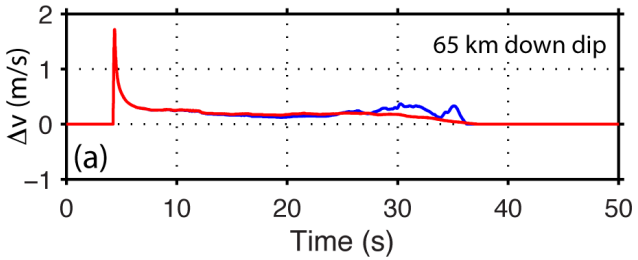

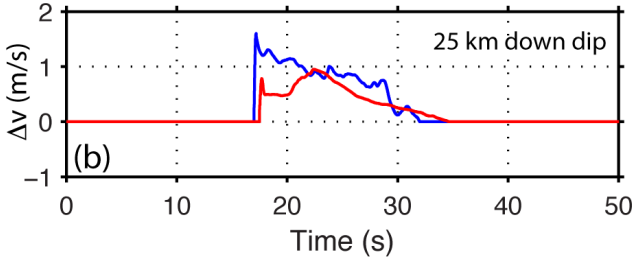

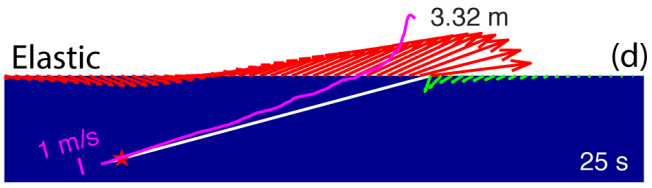

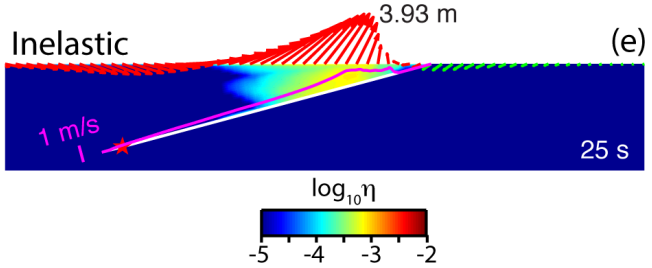

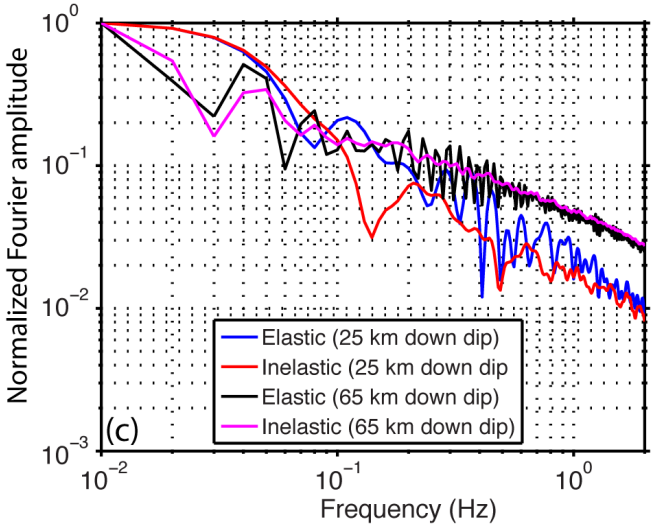

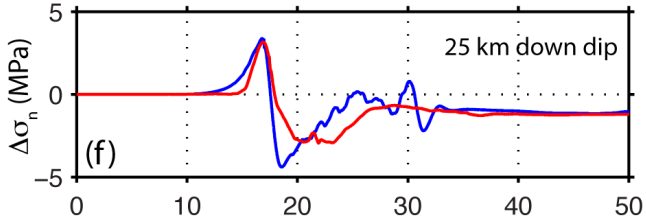

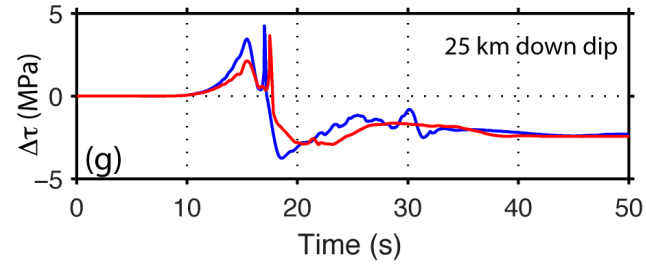

- More gradual stress change
- Smoother slip velocity
- Less high-frequency radiation

Moment Rate Time Functions and Spectra

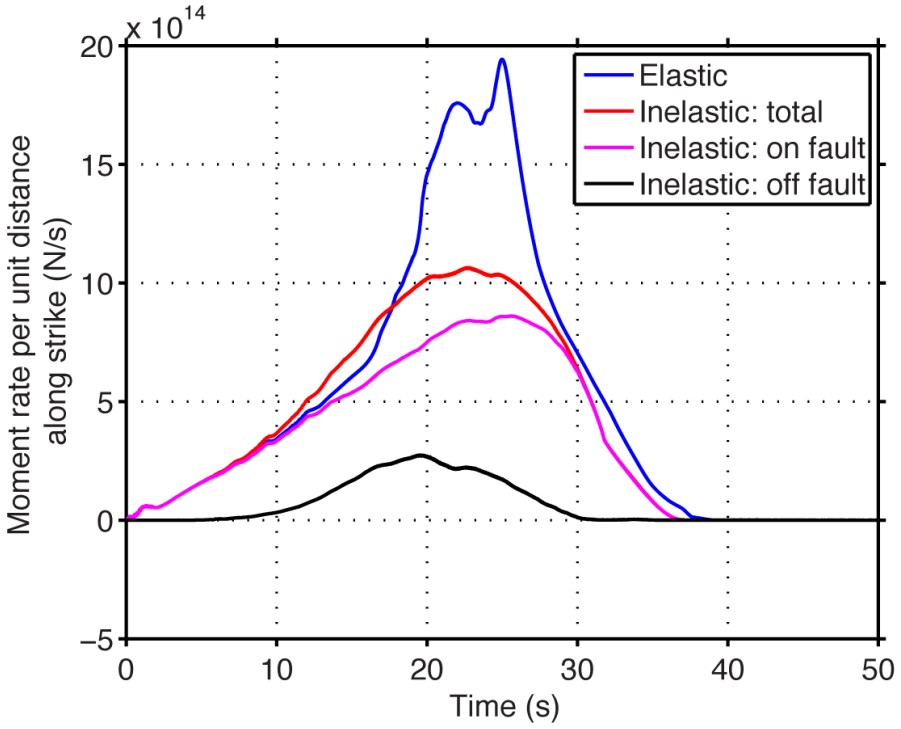

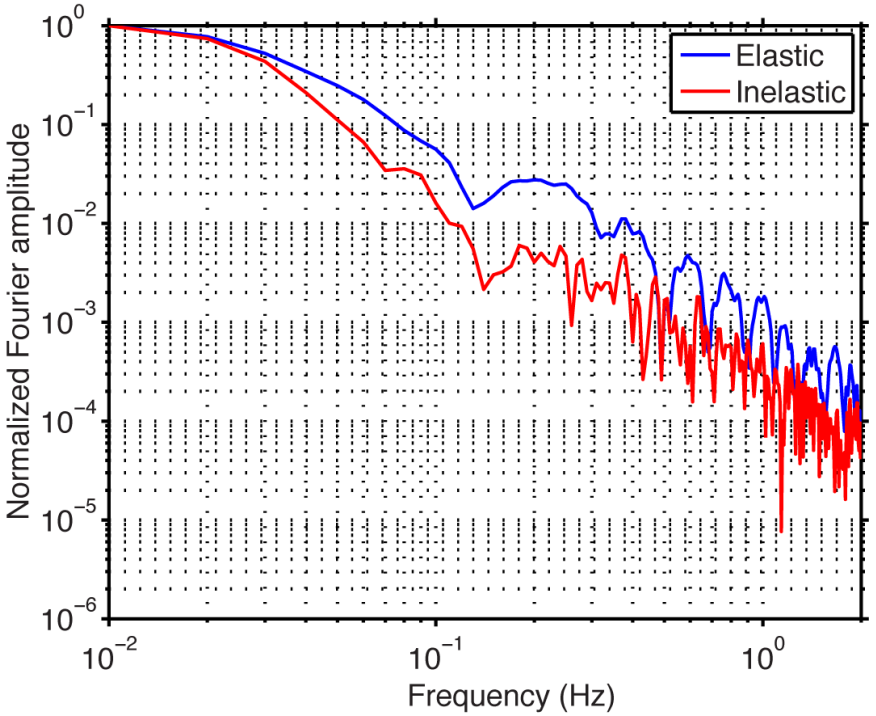

Less high-frequency radiation!

16 August 2005 Miyagi-oki
Mo= 0.9 x 10^{20} Nm (M_W = 7.2)
Depth 36 km

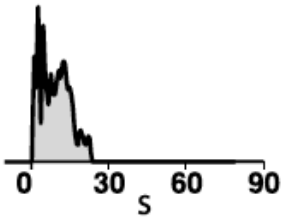

centroid time 9.7 s

9 March 2011 Tohoku-oki
Mo = 1.9 x 10^{20} Nm (M_W = 7.5)
Depth 14 km

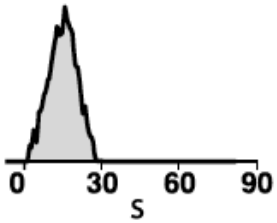

centroid time 14.3 s

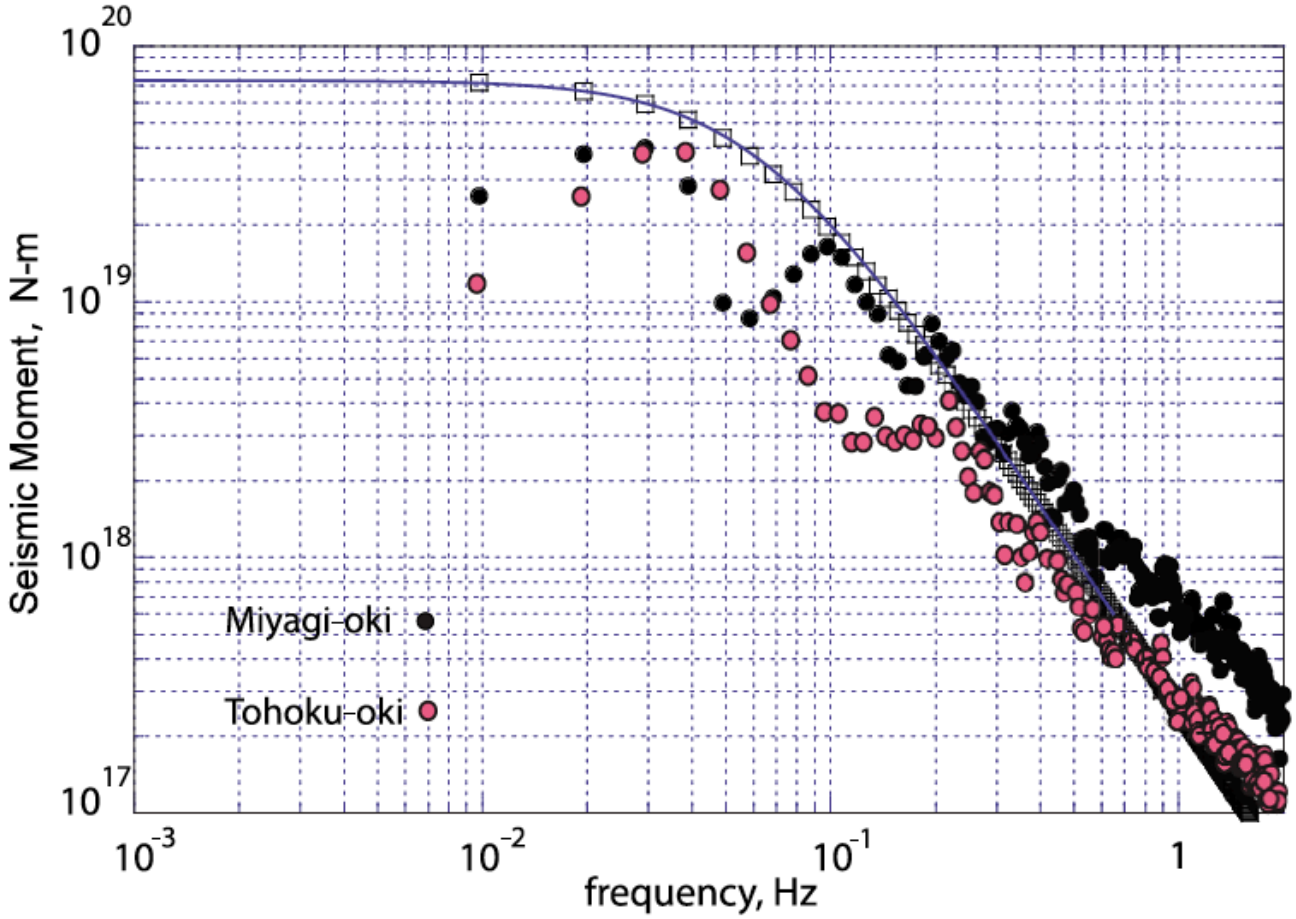

Lay et al. (2012)

Moment-Scaled Radiated Energy

moment contributor

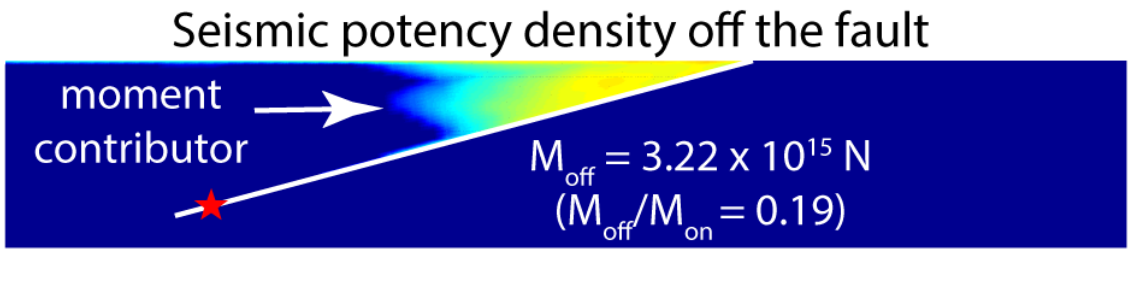

energy sink

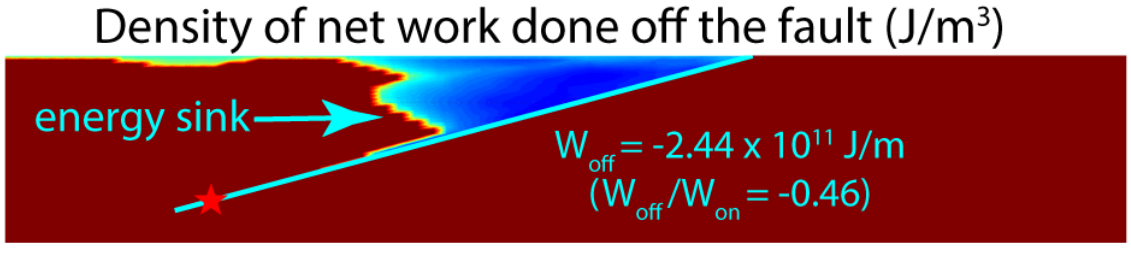

Elastic

M: 2.52 x 10^{16} N
E^R: 6.12 x 10^{11} J/m
E^R/M: 2.43 x 10^{-5}

Inelastic

M: 1.99 x 10^{16} N
E^R: 2.91 x 10^{11} J/m
E^R/M: 1.46 x 10^{-5}

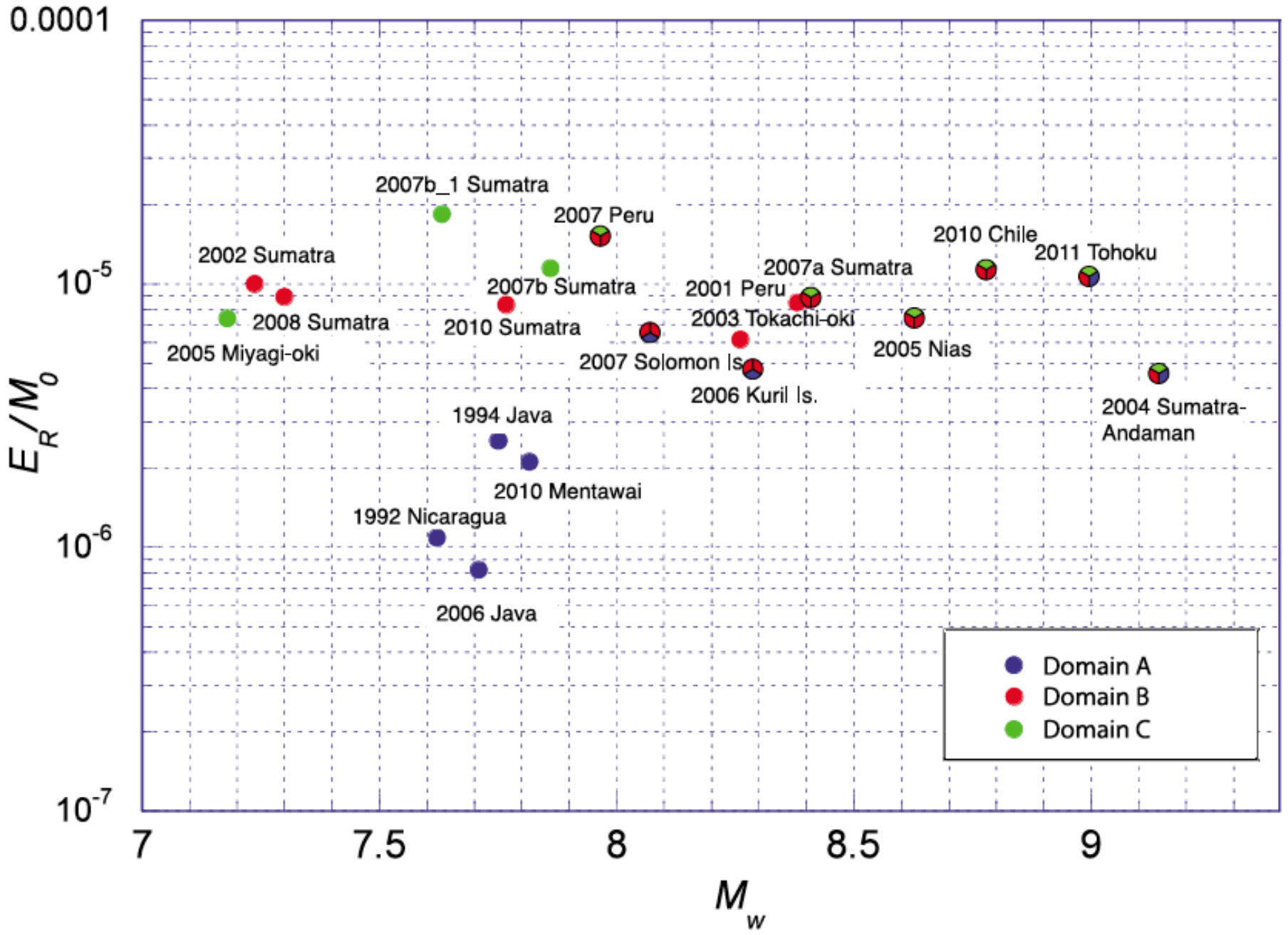
0.0001
10^{-5}
10^{-6}
10^{-7}
E_R/M_0
7
7.5
8
8.5
9
M_w
2007b_1 Sumatra
2007 Peru
2002 Sumatra
2007b Sumatra
2010 Chile
2011 Tohoku
2007a Sumatra
2001 Peru
2008 Sumatra
2010 Sumatra
2003 Tokachi-oki
2005 Miyagi-oki
2007 Solomon Is.
2005 Nias
2006 Kuril Is.
2004 Sumatra-Andaman
1994 Java
2010 Mentawai
1992 Nicaragua
2006 Java
Domain A
Domain B
Domain C

Another Look at Subduction Zone Fault Geometry

Large seafloor uplift

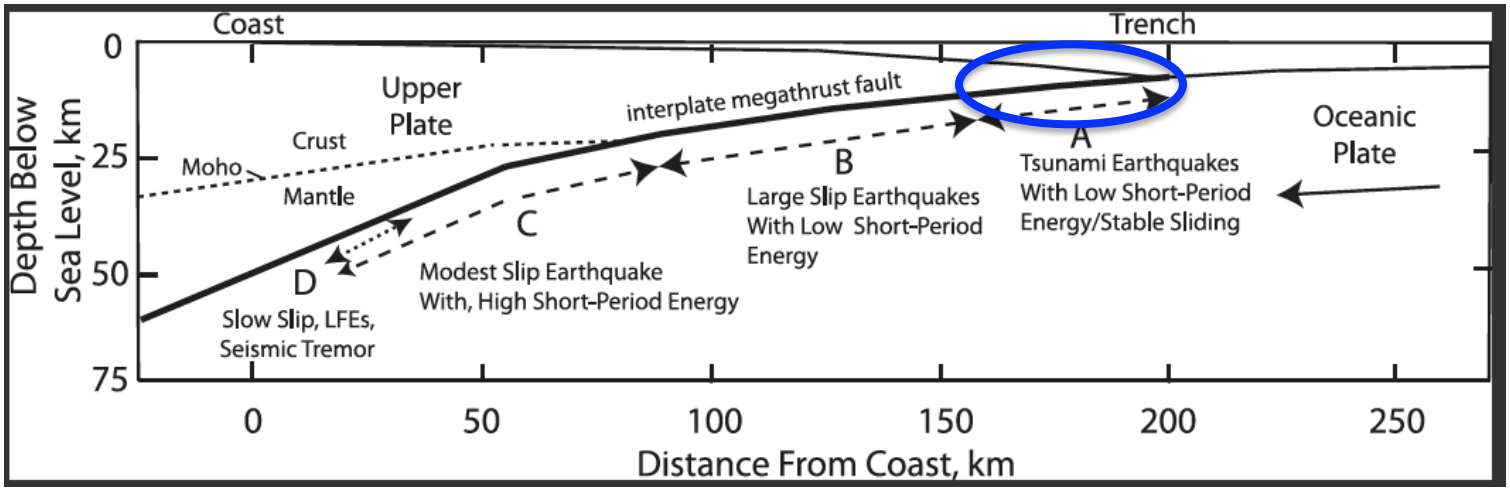

Shallower fault dip

↓

Smaller confining pressure

↓

Easier to fail

Larger seafloor uplift → Less high-frequency radiation

Coseismic Displacements for the 1964 Alaska Earthquake

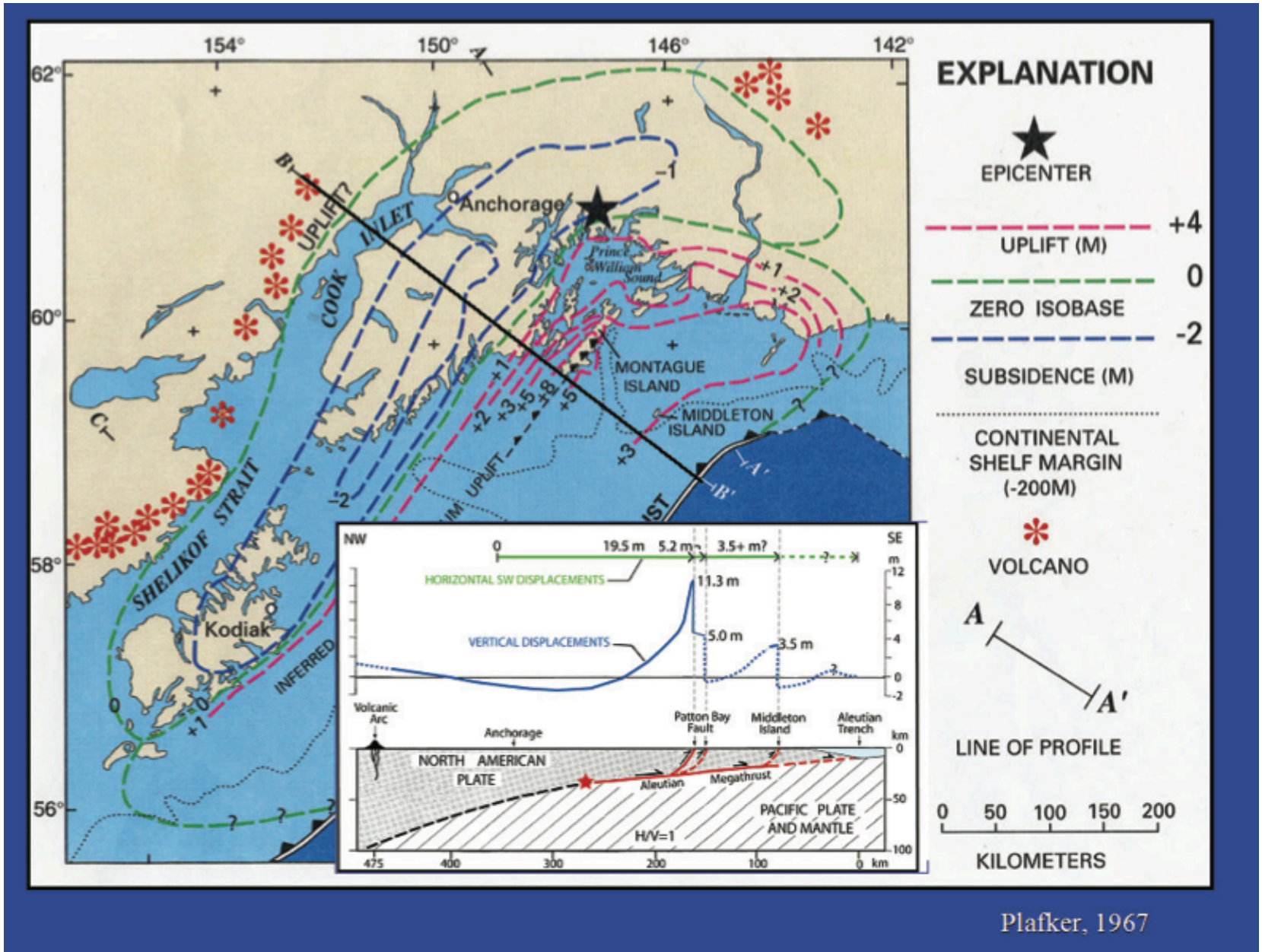

Plafker, 1967

Conclusions

Extensive Coulomb failure in the wedge provides a unifying interpretation to nearly all anomalous features of shallow subduction earthquakes, including:

- Slow rupture velocity
- Efficient tsunami generation
- Deficiency in high-frequency radiation
- Low energy-to-moment ratio

Namazu